

# Studying the Effect of Site-Specific Hydrophobicity and Polarization on Hydrogen Bond Energy of Protein Using a Polarizable Method

Chang G. Ji,<sup>\*,†,‡</sup> Xudong Xiao,<sup>†,‡</sup> and John Z. H. Zhang<sup>\*,†,‡,§</sup>

<sup>†</sup>State Key Laboratory of Precision Spectroscopy, Department of Physics, East China Normal University, Shanghai 200062, China

<sup>‡</sup>Institute of Theoretical and Computational Science, Institute for Advanced Interdisciplinary Research, East China Normal University, Shanghai 200062, China

<sup>§</sup>Department of Chemistry, New York University, New York, New York 10003, United States

## S Supporting Information

**ABSTRACT:** Quantification of backbone hydrogen bond energies in protein folding has remained elusive despite extensive theoretical and experimental investigations over the past 70 years. This is due to difficulties in experimental mutagenesis study as well as the lack of quantitatively reliable methods in theoretical calculation. Recent advance in experiment has enabled accurate measurement of site-specific backbone hydrogen bond energy in protein. In the present work, we developed an accurate and practical polarizable method to study site-specific hydrogen bond energies in the PIN WW domain. Excellent quantitative agreement between our calculated hydrogen bonding energy and recent experimental measurement is obtained. The direct comparison between theory and experiment helps uncover the microscopic mechanism of experimentally observed context dependent hydrogen bond contribution to protein stability in beta-sheet. In particular, our study reveals two effects that act in a cooperative manner to impact the strength of a hydrogen bond. One is the dynamic stability of the hydrogen bond determined by nearby solvent molecules, and the other is the polarization state of the hydrogen bond influenced by local electrostatic environment. The polar character of the hydrogen bond results in strong coupling between hydrophobic and polarization interactions in a cooperative manner. This nonadditive character in hydrogen bonding should help us better understand the microscopic mechanism in protein folding. Our study also investigated the possible structural effect of backbone amide to ester mutation which should be helpful to experimentalists using this technique in mutagenesis study.

## INTRODUCTION

The “protein folding problem” is the Holy Grail in biochemistry research.<sup>1,2</sup> Uncovering the energetic contribution of folded structure is a key to our understanding of the folding problem.<sup>3</sup> Hydrophobic effect and hydrogen bond (HB) interactions are recognized as the two most important forces that drive a protein into folded structure from random states.<sup>4</sup> Due to its important role in many biological processes such as in enzyme reaction, protein–ligand binding and signal transduction, study of hydrogen bonds has attracted much experimental and theoretical interests.<sup>3,5</sup>

Whether intraprotein hydrogen bonds energetically stabilize or destabilize a folded structure<sup>5</sup> is one of the central issues in protein folding study. To further complicate the issue, different experiments have given different conclusions. Klotz and Farnham suggested that formation of intraprotein hydrogen bond is an energetically disfavored process<sup>6</sup> in an aqueous environment based on their dimerization experiment of N-methyl acetamide (NMA) monomers. However, Baldwin and co-workers showed that a short poly alanyl peptide can form stable helix in water, implying that a hydrogen bond contributes to the stability of protein.<sup>7</sup> On the other hand, theoretical studies by Honig and co-workers concluded that a hydrogen bond does not contribute energetically to helix stability due to a large desolvation penalty in forming intraprotein hydrogen bonds.<sup>8–10</sup> Instead, they suggested that hydrogen bonds may help the packing of folded protein structure and maximize the van de Waals interactions in protein. However, Anbelj and Baldwin suggested that

simple NMA based experiments could not be a suitable model system for studying the energetics of hydrogen bonds in protein folding because nearby residue types may have influence on the strength of the hydrogen bond. Thus, the issue whether a hydrogen bond contributes positively or negatively to protein stability remains elusive.

Some studies suggest that contribution of a hydrogen bond to protein stability depends on the polarity of hydrogen bond's microenvironment.<sup>11–13</sup> Recent backbone mutation studies by Kelly and co-workers<sup>14–16</sup> have shown that hydrogen bonds' contribution to folding energetics is context dependent. Based on the quantitative measurement of hydrogen bond strength in their double mutation experiments, Gao et al. suggested that a hydrogen bond is much stronger in a nonpolar microenvironment than in a polar one.<sup>17</sup> However, mutations may be accompanied by structural changes, which could confound the experimental results.<sup>18,19</sup> Thus, the molecular origin of a macroscopically observed difference in hydrogen bond strength is difficult to access. An alternative but complementary approach to direct experimental measurement is to use computational methods at atomic resolution.<sup>20</sup> Molecular simulations can quantify individual interaction elements directly, without introducing any structural perturbation.

Since current standard force fields are nonpolarizable and unable to describe the polarization effect,<sup>21</sup> they fail to capture

Received: March 28, 2012

Published: May 11, 2012



environment-dependent character of hydrogen bond energy. In a previous study,<sup>22</sup> we investigated strength of a single hydrogen bond using polarized protein specific charge in MD simulation. In that approach, atomic charges were updated during MD simulation through quantum mechanical calculation.<sup>22–26</sup> However, repeated quantum mechanical calculation is computationally demanding for molecular dynamics simulation. Here we develop a new polarizable charge model (semifluctuating charge model) to investigate the origin of the position dependent and microenvironment dependent character of hydrogen bond energy.<sup>14,15,17</sup> The environment-dependent charge (EDC) model was developed for MD simulation to account for the polarization effect. The EDC parameters are derived from large sets of quantum electronic structure calculation of model systems in gas phase and in solution. Polarization effect is explicitly included in the simulation since charges used were updated frequently according to the local electrostatic environment during the simulation. Here we focus our study on the backbone hydrogen bonds in the WW domain of PIN, which was experimentally studied by Kelly and co-workers.<sup>15,17</sup> We study the dynamic and energetic properties of backbone hydrogen bonds under different positions and the influence of microenvironment on hydrogen bond strength achieved through computational mutation of side chains. Besides, amide to ester mutation, which was extensively used in experiments in studying elementary interactions in proteins, was also investigated to help us understand experimental protocols more thoroughly.

## THEORETICAL METHODS

**1. Semifluctuating Charge Model.** It was well recognized that electrostatic interaction was the dominant contributor of hydrogen bond interactions.<sup>7,27</sup> Polar groups such as NH and CO in protein backbone all have polarizable dipoles. The strength of electrostatic interaction strongly depends on the polarization state of those dipoles. Traditional classic force fields using fixed partial charge model is incapable of describing variable polarization state of those dipoles under different microenvironment. Since electrostatic interaction plays an essential role in many biological processes and is a key factor in protein/drug binding, a lot of efforts have been made incorporating polarization effects in molecular simulation. A number of representative approaches include induced point dipole model,<sup>28</sup> fluctuating charge model,<sup>29,30</sup> Drude oscillator model,<sup>31</sup> and electronic structure based force field.<sup>32</sup> However, there is still no consensus on which approach is generally applicable.<sup>21</sup> Here we propose a simple fluctuating charge model based on large scale QM/MM calculation on the model system to investigate backbone hydrogen bond strength in protein. In this model, only charges of backbone NH and CO groups of the protein are allowed to fluctuate during MD simulation. For this reason, we call this model the semifluctuating charge model.

Let us consider a simple polar molecule: CH<sub>3</sub>COCH<sub>3</sub>. This molecule will be polarized when placed in an electric field. This polarization will generate two opposing effects in energy. On one hand, the polarization will enhance the interaction energy between the molecule and the external electric field in order to lower the system energy. On the other hand, the internal energy of the molecule will be increased as a result of distortion of the electron charge distribution of the molecule due to polarization. This energy was usually called distortion energy in *ab initio* quantum mechanical calculations. Berendson called this term “missing term in effective pair potential”,<sup>33</sup> which

refers to this as “the positive self-energy representing the energy it costs to distort a molecule to its polarized state”. Distortion energy was a liability of the polarization process. When a polar molecule is moved from vacuum to liquid phase, these two opposing energetic effects will counter balance each other to establish an equilibrium (the lowest energy state) when the molecule reaches its correctly polarized state under a given electric field generated by surrounding molecules.

Here we use this rationale to find the relationship between the distortion energy and polarization state under an external electric field. This was modeled by sampling different configurations of water around CH<sub>3</sub>COCH<sub>3</sub>. The CH<sub>3</sub>COCH<sub>3</sub> molecule was solvated in an octahedron-like TIP3P water box. A 30 ns NPT MD simulation was performed to simulate different external environments while the solute was kept fixed. A total of 15,000 configurations were extracted from the sampling simulation. For each configuration, an electronic structure of the solute was calculated with and without influence of the background charge to mimic gas phase and liquid phase environments, respectively. The polarization cost of transferring CH<sub>3</sub>COCH<sub>3</sub> from gas phase to liquid phase can be calculated using the following procedure.

The Schrodinger equations that describe electronic motion in gas phase and in solvent are, respectively

$$H_0\Psi_0 = E_0\Psi_0 \quad (1)$$

and

$$(H_0 + H')\Psi = E\Psi \quad (2)$$

where  $H_0$  is the solute Hamiltonian in gas phase, and  $H'$  is the interaction between the solute and the surrounding charges (atomic charges of background water molecules)

$$H' = \sum_{s,\alpha} \frac{q_s Z_\alpha}{|r_s - R_\alpha|} - \sum_{s,i} \frac{q_s}{|r_s - r_i|} \quad (3)$$

where  $q_s$  and  $r_s$  are, respectively, solvent charges, and their positions,  $Z_\alpha$  and  $R_\alpha$  are nuclear charges and their corresponding coordinates.

The polarization cost (or wave function distortion) energy is given by

$$E_{p-\text{cos } t} = \langle \Psi | H_0 | \Psi \rangle - \langle \Psi_0 | H_0 | \Psi_0 \rangle \quad (4)$$

Since we want to derive the polarization parameter for the CO group, the contribution from the two methane molecules was subtracted. Distortion energy of the CO group due to solvent's polarization can be calculated as

$$\Delta E_{p-\text{cos } t}^{\text{CO}} \approx E_{p-\text{cos } t}^{\text{CH}_3\text{COCH}_3} - E_{p-\text{cos } t}^{\text{CH}_4} - E_{p-\text{cos } t}^{\text{CH}_4} \quad (5)$$

And accordingly, change of CO group's dipole moment during this process can be calculated as

$$\Delta \mu^{\text{CO}} \approx \Delta \mu^{\text{CH}_3\text{COCH}_3} - \Delta \mu^{\text{CH}_4} - \Delta \mu^{\text{CH}_4} \quad (6)$$

The coordinates of the two methane molecules used in quantum mechanical calculation were extracted from the CH<sub>3</sub>COCH<sub>3</sub> molecule, and the background charges used to represent solvent molecules were the same as those used for the CH<sub>3</sub>COCH<sub>3</sub> molecule. Although this approach is not exact, it provides a good approximation. All the quantum mechanical calculations were performed with Gaussian09 software with the DFT method<sup>34</sup> (M06/6-31G\*\*).

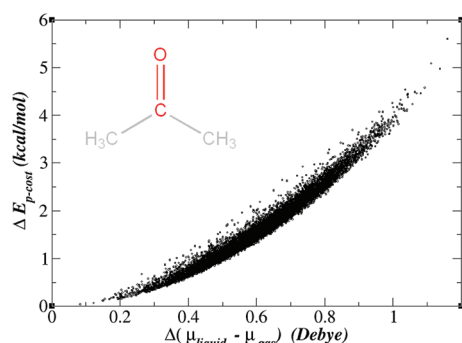


**Figure 1.** Distortion energy of the CO group as a function of dipole moment change.

Figure 1 shows the relationship between distortion energy and dipole moment of the CO group. The data in Figure 1 can be fitted into quadratic relation

$$\Delta E_{p-\text{co}} = k(\mu_{\text{liquid}} - \mu_{\text{gas}})^2 \quad (7)$$

Now consider transferring a polar group CO into an electric field, the energy of the system can be written as

$$\begin{aligned} E &= E_{\text{self}} + E_{\text{ele}} \\ &= [E_0 + k(\mu_{\text{liquid}} - \mu_{\text{gas}})^2] + [q_C \Phi_C + q_O \Phi_O] \end{aligned} \quad (8)$$

where  $q_C$  and  $q_O$  are, respectively, the atomic charge of the C and O atoms of the CO group.  $\Phi_C$  and  $\Phi_O$  are, respectively, the electrostatic potential at the C and O atoms. Thus when the gas phase CO group is placed in the liquid phase, the polarization process can be represented as transferring partial charge from one atom to the other. If charge transfer from atom O to atom C is  $\Delta q$ , then the final charge is

$$q_C = q_C^0 + \Delta q \quad (9)$$

$$q_O = q_O^0 - \Delta q \quad (10)$$

where  $q_C$  and  $q_O$  are, respectively, the atomic charge of the C and O atoms. Thus the change of dipole moment is

$$\mu_{\text{liquid}} - \mu_{\text{gas}} = \Delta q d_{\text{CO}} \quad (11)$$

where  $d_{\text{CO}}$  is the bond length of the C=O bond. Then eq 8 can be expressed as

$$E = E_0 + k(\Delta q d_{\text{CO}})^2 + (q_C^0 + \Delta q)\Phi_C + (q_O^0 - \Delta q)\Phi_O \quad (12)$$

By minimizing eq 12 with respect to variation of  $\Delta q$

$$\frac{\partial E}{\partial \Delta q} = 0 \quad (13)$$

we obtain the charge transfer along the CO bond under a given electrostatic potential

$$\Delta q = \frac{(\Phi_O - \Phi_C)}{2d_{\text{CO}}^2 k} \quad (14)$$

In the current study, we only consider the polarization of the backbone NH and CO groups as they are the critical components of intraprotein hydrogen bonds. The NH and CO groups are polarized independently, since unphysical characteristics arise when charge transfer is allowed among all chemical

bonds.<sup>35,36</sup> To best mimic quantum calculated polarized charges of  $\text{CH}_3\text{CONHCH}_3$  in solvent, the parameters  $q^0$  were optimized, and their optimized values are listed in Table 1.

**Table 1.** Numerically Determined Parameters of the Semifluctuating Charge Model

|          | $k$ (kcal/mol-debye <sup>2</sup> ) |        | $q^0$  |
|----------|------------------------------------|--------|--------|
| C=O bond | 4.14                               | 0.602  | −0.504 |
| N–H bond | 11.7                               | −0.364 | 0.261  |

Since only part of the protein is polarized during the simulation, we name this approach semifluctuating charge model. In our MD simulation, the charges of the backbone NH and CO groups were updated every 100 steps (about 100 fs). Compared to traditional fixed charge model, our new model adds about 1% extra computational time but captures the most essence of the polarization effect in protein's hydrogen bonds.

**2. System Buildup and MD Simulation.** The initial configuration of the PIN WW domain was taken from the crystal structure with Protein Data Bank ID code 1PIN.<sup>37</sup> The protein system is solvated in an octahedron-like TIP3P water box and is neutralized by adding counterions. Periodic boundary conditions and the Particle Mesh Ewald<sup>38</sup> methods were used to treat long-range electrostatic effects. Each system is relaxed in 10,000 steps with constraint on protein, followed by full minimization without any constraints. For MD simulation, integration time step is 1 fs. The temperature is regulated using Langevin dynamics with the collision frequency set to 2 ps<sup>−1</sup>. All the covalent bonds involving hydrogen atoms are fixed by applying the SHAKE algorithm.<sup>39</sup> After heating and equilibration, the production MD simulation was performed at 300K (NPT). Amber99SB force field<sup>40</sup> was used for proteins. A semifluctuating charge model was applied to backbone NH and CO groups. In the current simulation study, a modified version of the Amber10 package is used as a computational tool.<sup>41</sup> During the simulation, electrostatic potentials on each atom were stored, and polarized charges of the amide NH and CO groups were updated according to a time-averaged electrostatic potential over each 100 time step period (see Figure 2).

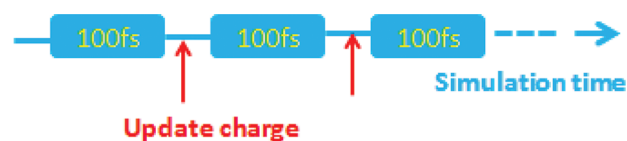


**Figure 2.** Schematic description of simulation protocol.

## RESULTS AND DISCUSSION

**1. Position Dependent Strength of Hydrogen Bond.** In this study, 20 ns MD simulation was performed for the production run, and trajectories and charges were saved every 1 ps, resulting in 20,000 snapshots for further analysis in each simulation.

Figure 3 shows the average atomic charge of the backbone NH and CO groups of each residue as a function of position along the peptide chain. Clearly, these two atomic charges differ a lot under different environments, underlying the importance of polarization. Charge of the C atom of the backbone CO group is in the range of 0.6 to 0.8 and that of the N atom is in

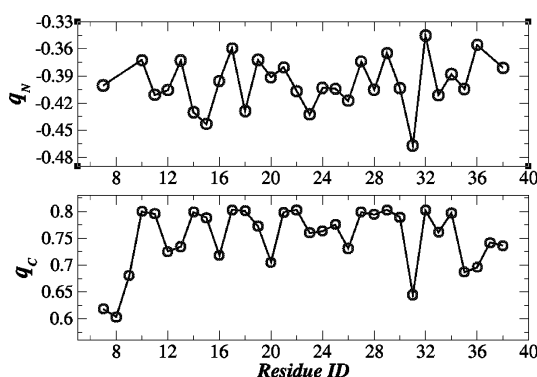


**Figure 3.** Average atomic charges of the backbone NH and CO groups of all the residues of the wild type PIN WW domain.

the range of  $-0.35$  to  $-0.46$ . This result clearly reflects the fact that each polar site has a specific polarization state, determined by a unique electrostatic environment formed by nearby protein residues and solvents. Taking into account the polarization effect due to environment is critical to quantitatively determine the electrostatic interaction energy from computer simulation.

Crystal structure shows that 11 backbone hydrogen bonds exist in the PIN WW domain (details can be seen from Figure 4

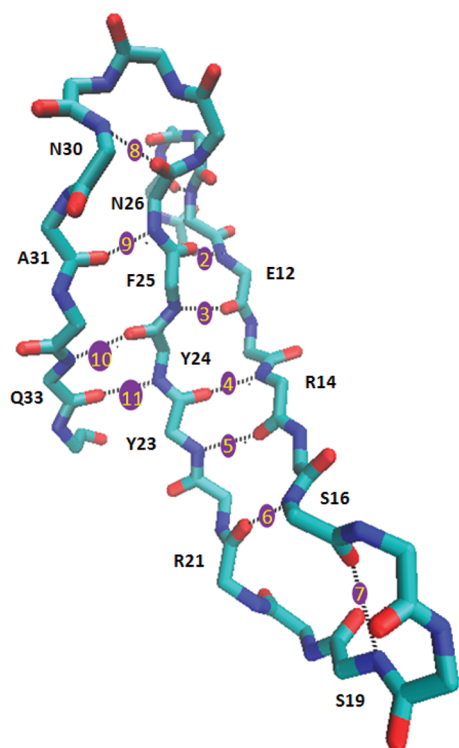


**Figure 4.** Backbone of beta-sheet region of the PIN WW domain (PDB code: 1PIN) where hydrogen bonds were shown in dotted lines. The hydrogen bonds are indicated by yellow numbers.

and Table 2). Here, the strength of those hydrogen bonds was calculated by configuration sampling from MD simulation. The strength of the hydrogen bond is determined by direct nonbonding electrostatic interactions between NH and CO groups

**Table 2.** Details of Eleven Backbone Hydrogen Bonds and Their Averaged Hydrogen Bond Lengths for the Wild Type PIN WW Domain

| HB index | donor (NH) | acceptor (CO) | Hbond length (Å) |
|----------|------------|---------------|------------------|
| HB1      | W11        | P9            | 2.80             |
| HB2      | E12        | F25           | 1.84             |
| HB3      | F25        | E12           | 1.87             |
| HB4      | R14        | Y23           | 1.88             |
| HB5      | Y23        | R14           | 1.86             |
| HB6      | S16        | R21           | 2.05             |
| HB7      | S19        | S16           | 2.82             |
| HB8      | N30        | N26           | 2.64             |
| HB9      | N26        | A31           | 1.97             |
| HB10     | Q33        | Y24           | 1.92             |
| HB11     | Y24        | Q33           | 1.87             |

$$E_{hb} = \frac{q_N q_C}{r_{NC}} + \frac{q_N q_O}{r_{NO}} + \frac{q_H q_C}{r_{HC}} + \frac{q_H q_O}{r_{HO}} \quad (15)$$

where  $q_N$ ,  $q_H$ ,  $q_C$ , and  $q_O$  are partial charge on N, H, C, O atoms, respectively. Specially, charges on the backbone NH and CO groups fluctuate with the change of environment.

Figure 5 plots the time evolution of the energy of two hydrogen bonds during MD simulation. Since the hydrogen

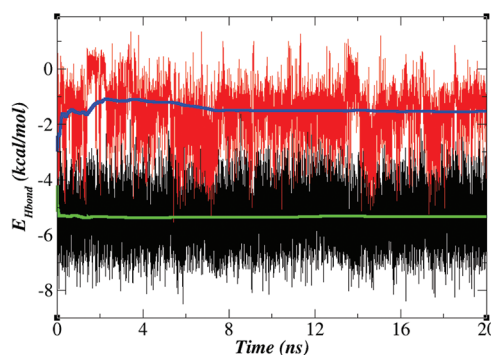


**Figure 5.** Hydrogen bond energy plotted as a function of simulation time for two hydrogen bonds (black: between NH@Tyr23 and CO@ARG14; red: between NH@SER19 and CO@SER16). The average H-bond energy is shown in green and blue lines, respectively.

bond length fluctuates (over 2 kcal/mol in energy fluctuation), a large amount of sampling is needed to obtain a stable result as shown in Figure 5. The converged HB strength for all 11 hydrogen bonds were plotted in Figure 6. One can see that the converged HB strength ranges from  $-1.5$  kcal/mol to  $-5.3$  kcal/mol. Four of them (HB1, HB7, HB8, HB9) were relatively weak (less than  $-3.4$  kcal/mol). Those four weak hydrogen bonds were all located in loop regions and exposed to solvents. During MD simulation, they were not so stable due to hydrogen bond competition from water molecules. From averaged hydrogen bond length listed in Table 2, we may find that the HB lengths for those four weak ones were relatively longer than others. Figure 5 (red line) also shows that HB7 breaks from time to time during the simulation. The other seven stronger hydrogen bonds were all located in a hydrophobic environment. The averaged hydrogen bond length for them is shorter and more stable during the MD simulation. There are still some minor differences between these strong hydrogen bonds. Although they all were buried under a hydrophobic environment, their polarization states were different.



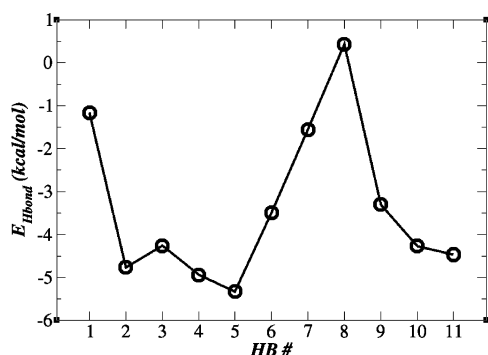


**Figure 6.** Average energy of each hydrogen bond of the wild type PIN WW domain.

This can be seen from averaged charges plotted in Figure 3. Different polarization states can be responsible for over 1 kcal/mol difference in energy for hydrogen bonds with the same geometry due to the polarization effect.

These results suggest that two elements are important in determining the strength of hydrogen bonds. One element is dynamic stability of the hydrogen bond in solvent. Hydrogen bond was not static in protein. Crystal structure observed hydrogen bonds may not be stable or even not exist in solvent environment. A recent NMR titration experiment<sup>42</sup> by Tomlinson et al. has shown that none of the hydrogen bonds formed between surface acidic and basic residues in the Protein GB1 domain in the crystal structure actually exists in the water environment. This may also partly explain why simple NMA based experiments may not be a suitable model for studying energetics of hydrogen bonds. The hydrogen bond formed between NMA is dynamically unstable due to water's competition. However, due to a cooperative effect, many hydrogen bonds in proteins are dynamically stable. The other element is that the polarization state of the hydrogen bond determined by an electrostatic environment created by other residues and solvents is essential for its strength. These two factors form the microscopic origin of the site-specific character of a protein hydrogen bond, and they act in a cooperative manner.

**2. Mutation of V22A.** In order to gain a further understanding of how a local environment influences the strength of a hydrogen bond, mutations of side chain on specific residues were performed to model change of a local environment. Kelly and co-workers quantitatively determined such energy change through double mutation experiments<sup>17</sup> (backbone amide to ester and V22 side chain mutation). However, experimental amide to ester mutation may introduce extra structure change to the original folded native structure. Thus, assigning the folding energy difference to a single hydrogen bond should be made with care. A computational approach could detect an energy change of a specific hydrogen bond directly without introducing perturbation to the original system.

In our calculation, we directly compare hydrogen bond strength of the HBs between the wild type PIN WW domain and the V22A form to investigate how minor local environment change influences protein's hydrogen energy. Val22 is a hydrophobic residue with a large side chain, which may form a large umbrella with other hydrophobic residues to protect nearby hydrogen bonds from being accessed by water molecules (see Figure 7). Mutation of this residue is an easy way to mimic "change of local environment" while keeping a

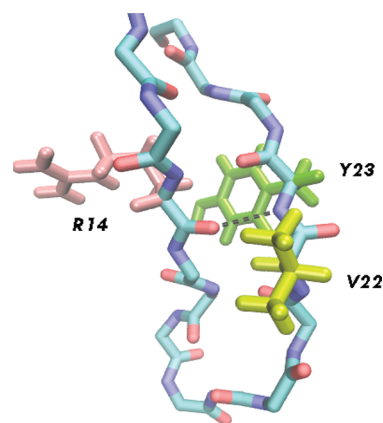


**Figure 7.** Structure of the Pin WW domain with a hydrogen bond formed between CO of Arg14 and NH of Tyr23 (The picture was generated from crystal structure. PDB ID: 1PIN).

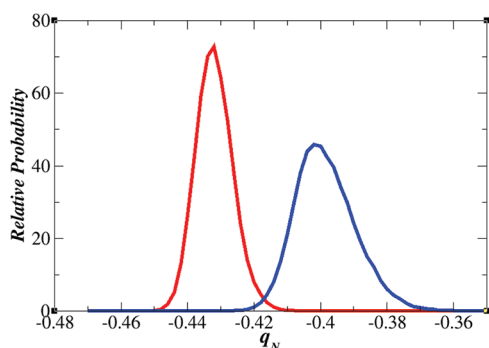
skeleton of the protein unchanged. Mutation of the Val to Ala would result in truncation of its large side chain to a small side chain. Thus a hydrogen bond nearby would lose "protection" from water and its polarization state will be changed, which can be evaluated directly.

Table 3 shows the comparison of hydrogen bond energy between the wild type and mutant. We can see from Table 3

**Table 3. Comparison of Hydrogen Bond Length (HBL) and Energy (HBE) of Backbone Hydrogen Bonds between the Wild Type and V22A Mutant of the PIN WW Domain**

| HB no.   | wild type |                | V22A mutant |                | $\Delta E$ |
|----------|-----------|----------------|-------------|----------------|------------|
|          | HBL(Å)    | HBE (kcal/mol) | HBL(Å)      | HBE (kcal/mol) |            |
| HB1      | 2.80      | -1.17          | 2.62        | -1.37          | -0.20      |
| HB2      | 1.84      | -4.75          | 1.85        | -4.69          | 0.05       |
| HB3      | 1.87      | -4.29          | 1.87        | -4.29          | 0.00       |
| HB4      | 1.88      | -4.95          | 1.89        | -4.84          | 0.11       |
| HB5      | 1.87      | -5.33          | 1.88        | -4.47          | 0.86       |
| HB6      | 2.05      | -3.48          | 2.02        | -3.36          | 0.12       |
| HB7      | 2.82      | -1.58          | 3.01        | -1.27          | 0.31       |
| HB8      | 2.64      | 0.39           | 2.70        | 0.36           | -0.04      |
| HB9      | 1.97      | -3.31          | 1.94        | -3.49          | -0.18      |
| HB10     | 1.92      | -4.30          | 1.94        | -3.96          | 0.35       |
| HB11     | 1.87      | -4.46          | 1.85        | -4.68          | -0.22      |
| $\Sigma$ |           | -37.21         |             | -36.06         | 1.15       |

that the lengths of these hydrogen bonds change little in general before and after the mutation. This implies that the side chain truncation of V22 does not change the main chain structure of the PIN WW domain. Also, the strengths of these HB do not change much except for the one near the V22 residue (HB5 in Table 3), which is the one formed between CO@arg14 and NH@Tyr23 (see Figure 7). The strength of this hydrogen bond changes from -5.33 kcal/mol to -4.47 kcal/mol upon mutation, with a reduction of 0.86 kcal/mol. Since the geometry of this hydrogen bond does not change much, the difference in energy mainly comes from change of polarization state under different microenvironments before and after the mutation. This was confirmed in Figure 8, in which distribution of the partial atomic charge of NH@Tyr23 during MD simulation was plotted. Figure 8 shows that NH@Tyr23 was less polarized after V22A mutation.



**Figure 8.** Distribution of partial atomic charge on backbone N atom in residue Tyr23 (red: wild type, blue: V22A mutant).

From the discussion given in the method section, especially through Figure 1 and eq 14, we know that the polarization state of a dipole is determined by the difference of electrostatic potential between the head and tail atoms of the dipole generated by the environment. Thus we plot the potential difference between the N atom and H atom of Tyr23 in Figure 9.

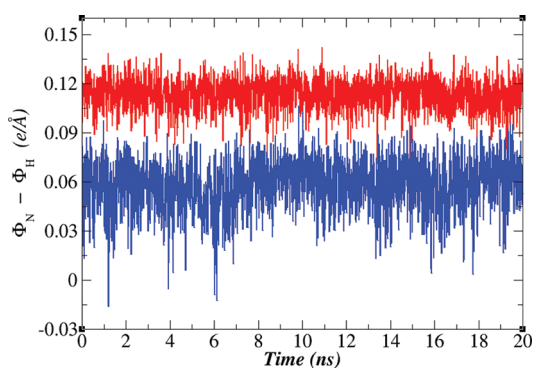


**Figure 9.** Difference of electrostatic potential between N atom and H atom of Tyr23 as a function of simulation time (red: wild type, blue: V22A mutant).

The average potential difference on N and H atoms of HN@Tyr23 is 0.113(e/Å) and 0.058(e/Å), respectively, for the native and V22A mutant. For the V22A mutant, the HB is more exposed to water, and water's screening effect is more pronounced compared to the native protein. This causes the potential difference on the N and H atoms smaller than that in the native form (in which this hydrogen bond was buried in a more hydrophobic environment). This is the origin of the different energetic contribution of hydrogen bond under different microenvironments.

Our simulation predicted a 1.15 kcal/mol reduction of the total HB energy of the V22A mutant (see Table 3). This finding is in excellent agreement with a previous double mutation experiment by Gao et al. in which they found an upper limit of 1.2 kcal/mol in the energy difference between the wild and mutant.<sup>17</sup>

Comparing the result predicted by MD simulation from the standard nonpolarizable force field can also be very informative. The calculated hydrogen bond energy is weaker when using the Amber force field due to the lack of polarization effect (see Table S1), and there is little difference in hydrogen bond energy between the wild type and the V22A mutant. Under the Amber force field, the atomic charges remain the same in both

the wild and mutant states, irrespective of the site specific microenvironment. This means that incorporation of the polarization effect in our study is critical.

These results suggest that environment is important in determining hydrogen bond's strength. Although the energy difference of 0.8 kcal/mol in a single hydrogen bond may not seem very large, consider that there may be hundreds of hydrogen bonds in a functional protein<sup>4</sup> and the collective effect could be significant. The free energy difference between folded and the unfolded states is often only a few kcal/mol for most of the proteins.<sup>4,5,43,44</sup> Each hydrogen bond has its specific polarization state due to the inhomogeneous character of protein. Thus accurate accounting of each hydrogen bond's strength in its proper electrostatic environment is imperative toward understanding the critical role of hydrogen bond in stabilizing protein's three-dimensional structure and other important biological processes.

Hydrogen bond interaction<sup>5</sup> and hydrophobic effect<sup>43</sup> are recognized as two of the most important driving forces in protein folding, but "which one is energetically dominating" has been a debated issue for the last 50 years.<sup>3,4,7,9,13,43,44</sup> Most experiments were based on single site mutation and model system study. They usually assign folding energy differences between wild and mutated form to a single factor, hydrophobic or hydrophilic. However, our simulation result and recent experimental backbone mutation studies<sup>15–17</sup> suggested that hydrogen bond strength is coupled to hydrophobic environment. Mutation of a single hydrophobic residue not only affects hydrophobic interaction in protein but also affects the energy of some neighboring hydrogen bonds. Using small representative organic molecules to model protein's elementary interactions may be improper because they neglect the many body effect or cooperativity that is very important in determining the thermodynamics of folding process. The polar character of hydrogen bond interaction and inhomogeneous protein environment are responsible for the nonadditive effect in protein folding.

**3. Effect of Backbone Amide to Ester Mutation.** Amide to ester mutation of the peptide bond was extensively used in biochemical studies.<sup>18</sup> Perturbation of the original nonbond interaction networks provides a useful tool for biochemists to investigate structure–function relationships. Predominant fact that amide to ester mutation in detecting energetics of hydrogen bond in protein folding is that such perturbation does not introduce an obvious structural change to the original interaction networks. However, such a hypothesis is rarely investigated. Here we try to explore the influence of amide to ester mutation on the strength of a backbone hydrogen bond and on the dynamic structure of the PIN WW domain (see Figure 10).

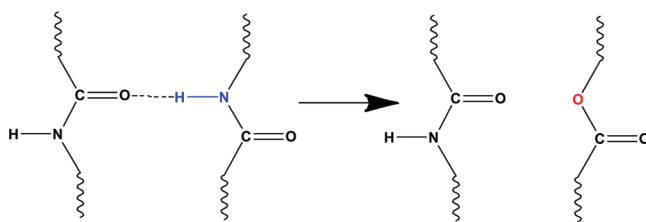


**Figure 10.** Amide to ester mutation disrupts backbone hydrogen bonds.

Table 4. Comparison of the HB Energy of the A2E Mutant and the Wild Type

|          | wild  | 11.A2E | 12.A2E | 14.A2E | 16.A2E | 19.A2E | 23.A2E | 24.A2E | 25.A2E | 26.A2E | 30.A2E | 33.A2E |
|----------|-------|--------|--------|--------|--------|--------|--------|--------|--------|--------|--------|--------|
| HB1      | -1.2  | -      | -1.0   | -0.6   | -0.8   | -0.6   | -0.9   | -0.9   | -1.5   | -0.5   | -1.0   | -1.5   |
| HB2      | -4.8  | -4.1   | -      | -4.2   | -4.2   | -4.0   | -4.2   | -4.2   | -3.9   | -2.7   | -4.2   | -4.7   |
| HB3      | -4.3  | -4.2   | -3.7   | -3.7   | -4.3   | -3.8   | -4.4   | -2.7   | -      | -4.4   | -4.2   | -3.9   |
| HB4      | -4.9  | -4.9   | -4.8   | -      | -5.1   | -5.1   | -3.5   | -4.0   | -4.8   | -5.0   | -4.9   | -4.9   |
| HB5      | -5.3  | -5.3   | -5.4   | -5.3   | -5.5   | -5.6   | -      | -5.4   | -5.4   | -5.4   | -5.3   | -5.3   |
| HB6      | -3.5  | -3.4   | -2.9   | -3.9   | -      | -2.7   | -0.7   | -3.6   | -3.2   | -3.5   | -3.1   | -3.7   |
| HB7      | -1.6  | -1.3   | -1.4   | -1.4   | -1.2   | -      | -1.0   | -1.5   | -1.4   | -1.4   | -1.5   | -1.5   |
| HB8      | 0.4   | 0.0    | 0.4    | 0.3    | 0.6    | 0.3    | 0.5    | 0.5    | 0.6    | -1.0   | -      | 0.7    |
| HB9      | -3.3  | -4.0   | -3.9   | -4.2   | -3.7   | -4.3   | -3.9   | -4.0   | -3.0   | -      | -4.3   | -3.6   |
| HB10     | -4.3  | -4.0   | -4.2   | -4.7   | -4.0   | -4.8   | -4.1   | -3.8   | -3.6   | -3.9   | -4.1   | -      |
| HB11     | -4.5  | -4.7   | -4.6   | -3.1   | -4.6   | -4.6   | -3.2   | -      | -4.5   | -4.7   | -4.4   | -4.1   |
| $\Sigma$ | -37.1 | -35.9  | -31.5  | -30.9  | -32.9  | -35.2  | -25.4  | -29.6  | -30.7  | -32.5  | -37.2  | -32.5  |
| $\Delta$ |       | 1.3    | 5.7    | 6.3    | 4.2    | 1.9    | 11.7   | 7.5    | 6.4    | 4.7    | -0.1   | 4.7    |

Eleven “amide to ester” (A2E) mutants were investigated, corresponding to all backbone hydrogen bonds studied here. The strength of each HB of those mutated proteins was listed in Table 4. For some of the A2E mutants, reduced total HB energy approximately equals to energy of the diminished hydrogen bond. Those mutants did not bring extra conformational change to the original protein structure. This implies that these mutations are structurally eligible. For some of the A2E mutants, reduced total HB energy is much larger than the energy of the diminished hydrogen bond (A2E mutant of R14, Y23, Y24, and F25). For those mutants, more than one hydrogen bond was affected due to mutation. For the Tyr23 A2E mutant, two of the hydrogen bonds near Tyr23 are also changed. From Table 4, we find that the strength of HB4 was reduced from  $-4.9$  kcal/mol to  $-3.5$  kcal/mol under Tyr23.A2E mutation. Similarly, the strength of HB6 was reduced from  $-3.5$  kcal/mol to  $-0.7$  kcal/mol. Time evolution of the hydrogen bond length of HB6 was plotted in Figure 11. As shown in Figure 11,

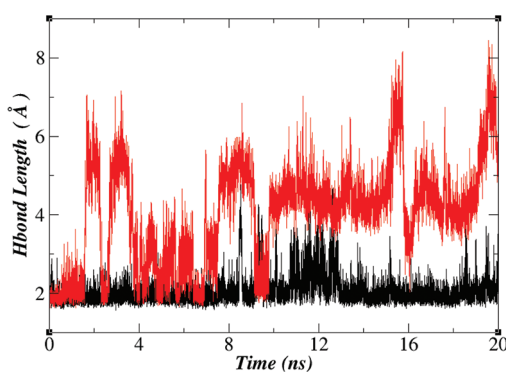


**Figure 11.** Hydrogen bond length of HB6 (between NH@S16 and CO@R21) as a function of simulation time. (black: wild type, red: Tyr23.A2E mutant).

this hydrogen bond was nearly broken during MD simulation for the Tyr23.A2E mutant. This implies that the local structure rearrangement occurs after amide to ester mutation of Tyr23. Comparison of the final structure of the Tyr23.A2E mutant with the wild type also confirmed that local structure around Tyr23 changed (see Figure 12). These findings suggest that not every secondary structural element can be subjected to eligible amide to ester mutation. The computational method may be helpful in experimental design of amide to ester mutation in

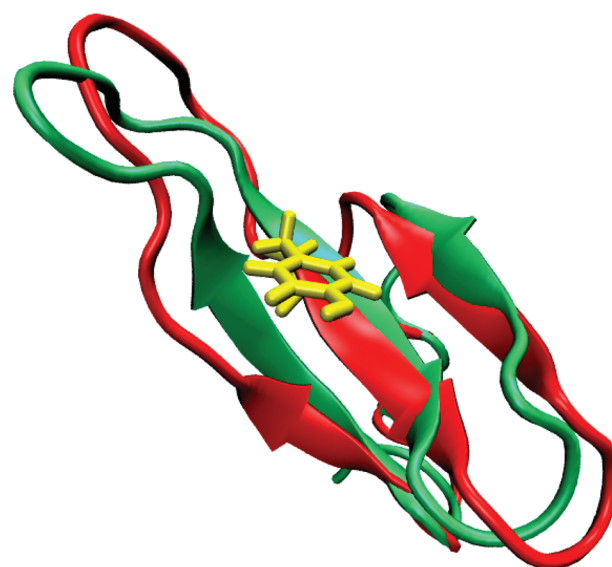


**Figure 12.** Superposition of final structure of Tyr23.A2E mutant (red) with wild type (green). Mutated Tyr23 was shown in yellow.

investigating hydrogen bond functionality in the biological process.

## CONCLUSION

Using MD simulation with a new semifluctuating charge method, the present study uncovered a microscopic mechanism of experimentally observed context dependent hydrogen bond contribution to protein stability. Two factors contribute to site-specific strength of hydrogen bonds in protein. One is the dynamic stability which was strongly influenced by solvents around the hydrogen bond. The other is the polarization state of the hydrogen bond which is influenced by local electrostatic environment. These two effects act in a cooperative manner. We successfully predicted experimentally observed hydrogen bond energy change due to mutation of the hydrophobic side chain of V22. The polar character of a hydrogen bond results in strong coupling between hydrophobic and hydrogen bond interactions. Most of the previous studies were focused on a single effect in protein folding. More attention needs to be paid to the coupling effect in future studies. The polarization related nonadditive effect revealed in the current study could trigger more experimental and theoretical studies along this line of thought to study the protein folding problem.

Through computational modeling, we also explored structural eligibility of amide to ester mutation on specific locations. Studies show that this kind of mutation may introduce extra structure change to the original folded structure and should be applied with care. Combined computational and experimental investigation on mutagenesis study in biochemical research is recommended.

Finally, we have provide a concise method in analyzing hydrogen bond strength in protein under a different environment which may facilitate further experimental and theoretical study on HB's role in protein folding and many other biological processes. Our polarizable charge model was computationally very efficient and adds only a little computational time compared to the traditional force field model. What is more, it captures most of the essence of the polarization effect in protein dynamics. It was built up on a simple physical picture of the "equilibrium between distortion energy up and interaction energy down" concept.

## ■ ASSOCIATED CONTENT

### ● Supporting Information

Hydrogen bond energies calculated with the Amber99SB force field are provided. This material is available free of charge via the Internet at <http://pubs.acs.org>.

## ■ AUTHOR INFORMATION

### Corresponding Author

\*C.G.J.: e-mail [chicago.ji@gmail.com](mailto:chicago.ji@gmail.com). J.Z.H.Z.: e-mail [john.zhang@nyu.edu](mailto:john.zhang@nyu.edu).

### Notes

The authors declare no competing financial interest.

## ■ ACKNOWLEDGMENTS

We thank the National Natural Science Foundation of China (Grants No. 21003048, 10974054, and 20933002). C.G.J. is also supported by "the Fundamental Research Funds for the Central Universities" and Open Research Fund of the State Key Laboratory of Precision Spectroscopy, East China Normal University. C.G.J. thanks Dr. John D. Chodera for his generous help on modifying the Amber source code. We also thank the Computer Center of ECNU for providing us computational time.

## ■ REFERENCES

- (1) Anfinsen, C. B. *Science* **1973**, *181*, 223.
- (2) Creighton, T. *Science* **1988**, *240*, 267.
- (3) Baldwin, R. L. *J. Mol. Biol.* **2007**, *371*, 283.
- (4) Pace, C. N. *Nat. Struct. Mol. Biol.* **2009**, *16*, 681.
- (5) Bolen, D. W.; Rose, G. D. *Annu. Rev. Biochem.* **2008**, *77*, 339.
- (6) Klotz, I. M.; Farnham, S. B. *Biochemistry* **1968**, *7*, 3879.
- (7) Baldwin, R. L. *J. Biol. Chem.* **2003**, *278*, 17581.
- (8) Yang, A.-S.; Hitz, B.; Honig, B. *J. Mol. Biol.* **1996**, *259*, 873.
- (9) Yang, A.-S.; Honig, B. *J. Mol. Biol.* **1995**, *252*, 351.
- (10) Yang, A.-S.; Honig, B. *J. Mol. Biol.* **1995**, *252*, 366.
- (11) Fernández, A.; Berry, R. S. *Biophys. J.* **2002**, *83*, 2475.
- (12) Fernández, A.; Zhang, X.; Chen, J. In *Progress in Molecular Biology and Translational Science*; Conn, P. M., Ed.; Academic Press: 525 B Street, Suite 1900, San Diego, CA, USA, 2008; Vol. 83, p 53.
- (13) Némethy, G.; Steinberg, I. Z.; Scheraga, H. A. *Biopolymers* **1963**, *1*, 43.
- (14) Deechongkit, S.; Dawson, P. E.; Kelly, J. W. *J. Am. Chem. Soc.* **2004**, *126*, 16762.
- (15) Deechongkit, S.; Nguyen, H.; Powers, E. T.; Dawson, P. E.; Gruebele, M.; Kelly, J. W. *Nature* **2004**, *430*, 101.

- (16) Jager, M.; Deechongkit, S.; Koepf, E. K.; Nguyen, H.; Gao, J.; Powers, E. T.; Gruebele, M.; Kelly, J. W. *Pept. Sci.* **2008**, *90*, 751.
- (17) Gao, J.; Bosco, D. A.; Powers, E. T.; Kelly, J. W. *Nat. Struct. Mol. Biol.* **2009**, *16*, 684.
- (18) Choudhary, A.; Raines, R. T. *ChemBioChem* **2011**, *12*, 1801.
- (19) Scheike, J. A.; Baldauf, C.; Spengler, J.; Albericio, F.; Pisabarro, M. T.; Koks, B. *Angew. Chem., Int. Ed.* **2007**, *46*, 7766.
- (20) Levitt, M. *Nat. Struct. Biol.* **2001**, *8*, 392.
- (21) Cieplak, P.; Dupradeau, F. Y.; Duan, Y.; Wang, J. M. *J. Phys.: Condens. Matter* **2009**, *21*, 333102.
- (22) Ji, C. G.; Zhang, J. Z. H. *J. Phys. Chem. B* **2011**, *115*, 12230.
- (23) Ji, C. G.; Zhang, J. Z. H. *J. Am. Chem. Soc.* **2008**, *130*, 17129.
- (24) Ji, C. G.; Zhang, J. Z. H. *J. Phys. Chem. B* **2009**, *113*, 13898.
- (25) Ji, C. G.; Zhang, J. Z. H. *J. Phys. Chem. B* **2009**, *113*, 16059.
- (26) Ji, C. G.; Mei, Y.; Zhang, J. Z. H. *Biophys. J.* **2008**, *95*, 1080.
- (27) Pauling, L.; Delbruck, M. *Science* **1940**, *92*, 77.
- (28) Cieplak, P.; Caldwell, J.; Kollman, P. *J. Comput. Chem.* **2001**, *22*, 1048.
- (29) Patel, S.; Brooks, C. L. *J. Comput. Chem.* **2004**, *25*, 1.
- (30) Patel, S.; Mackerell, A. D.; Brooks, C. L. *J. Comput. Chem.* **2004**, *25*, 1504.
- (31) Lamoureux, G.; MacKerell, J. A. D.; Roux, B. *J. Chem. Phys.* **2003**, *119*, 5185.
- (32) Xie, W.; Orozco, M.; Truhlar, D. G.; Gao, J. *J. Chem. Theory Comput.* **2009**, *5*, 459.
- (33) Berendsen, H. J. C.; Grigera, J. R.; Straatsma, T. P. *J. Phys. Chem.* **1987**, *91*, 6269.
- (34) Zhao, Y.; Truhlar, D. G. *Acc. Chem. Res.* **2008**, *41*, 157.
- (35) Banks, J. L.; Kaminski, G. A.; Zhou, R.; Mainz, D. T.; Berne, B. J.; Friesner, R. A. *J. Chem. Phys.* **1999**, *110*, 741.
- (36) Chelli, R.; Procacci, P.; Righini, R.; Califano, S. *J. Chem. Phys.* **1999**, *111*, 8569.
- (37) Ranganathan, R.; Lu, K. P.; Hunter, T.; Noel, J. P. *Cell* **1997**, *89*, 875.
- (38) Darden, T.; York, D.; Pedersen, L. *J. Chem. Phys.* **1993**, *98*, 10089.
- (39) Andersen, H. C. *J. Comput. Phys.* **1983**, *52*, 24.
- (40) Hornak, V.; Abel, R.; Okur, A.; Strockbine, B.; Roitberg, A.; Simmerling, C. *Proteins: Struct., Funct., Bioinf.* **2006**, *65*, 712.
- (41) Case, D. A.; Cheatham, T. E.; Darden, T.; Gohlke, H.; Luo, R.; Merz, K. M.; Onufriev, A.; Simmerling, C.; Wang, B.; Woods, R. J. *J. Comput. Chem.* **2005**, *26*, 1668.
- (42) Tomlinson, J. H.; Ullah, S.; Hansen, P. E.; Williamson, M. P. *J. Am. Chem. Soc.* **2009**, *131*, 4674.
- (43) Dill, K. A. *Biochemistry* **1990**, *29*, 7133.
- (44) Pace, C. N.; Hermans, J. *Crit. Rev. Biochem. Mol. Biol.* **1975**, *3*, 1.